Charging of moving surfaces by corona discharges sustained in air

Jun-Chieh Wang,[1,a)] Daihua Zhang,[2,b)] Napoleon Leoni,[3,c)] Henryk Birecki,[3,d)] Omer Gila,[3,e)] and Mark J. Kushner[1,f)]
[1]*Department of Electrical Engineering and Computer Science, University of Michigan, 1301 Beal Ave., Ann Arbor, Michigan 48109-2122, USA*
[2]*Tianjin University, Tianjin, China*
[3]*Hewlett-Packard Research Labs, Palo Alto, California 94304, USA*

(Received 7 May 2014; accepted 6 July 2014; published online 23 July 2014)

Atmospheric pressure corona discharges are used in electrophotographic (EP) printing technologies for charging imaging surfaces such as photoconductors. A typical corona discharge consists of a wire (or wire array) biased with a few hundred volts of dc plus a few kV of ac voltage. An electric discharge is produced around the corona wire from which electrons drift towards and charge the underlying dielectric surface. The surface charging reduces the voltage drop across the gap between the corona wire and the dielectric surface, which then terminates the discharge, as in a dielectric barrier discharge. In printing applications, this underlying surface is continuously moving throughout the charging process. For example, previously charged surfaces, which had reduced the local electric field and terminated the local discharge, are translated out of the field of view and are replaced with uncharged surface. The uncharged surface produces a rebound in the electric field in the vicinity of the corona wire which in turn results in re-ignition of the discharge. The discharge, so reignited, is then asymmetric. We found that in the idealized corona charging system we investigated, a negatively dc biased corona blade with a dielectric covered ground electrode, the discharge is initially sustained by electron impact ionization from the bulk plasma and then dominated by ionization from sheath accelerated secondary electrons. Depending on the speed of the underlying surface, the periodic re-ignition of the discharge can produce an oscillatory charging pattern on the moving surface. © *2014 AIP Publishing LLC*.
[http://dx.doi.org/10.1063/1.4890520]

I. INTRODUCTION

Atmospheric pressure plasmas are widely employed to functionalize surfaces due to their short treatment times, room temperature operation, and ability to operate without vacuum facilities. One such application is improvement in wettability of surfaces.[1–5] By creating new surface functional groups on commodity polymer sheets, metallic foils, and paper, surface tension (or surface energy, dyne/cm) can be increased to improve the bonding abilities with adhesives, coatings, and solvents. As a result, the printing quality and lamination strength can be improved. For example, commodity hydrocarbon polymeric materials such as polyethylene[1,5] and polypropylene[2–5] are hydrophobic and relatively chemically inert due to their low surface energy. A common process to improve wettability and adhesion of inks to these materials is through the use of oxygen containing electric discharges to affix oxygen to their surfaces. More recent developments in the use of atmospheric pressure discharges to change surface properties are in the biomedical field. Sterilization of biomedical devices and the creation of reactive surface functionalities to optimize the biocompatibility have been proven to benefit from atmospheric pressure plasmas.[6–9]

A natural outcome of atmospheric pressure discharges in contact with dielectric or low conductivity surfaces is charging of those surfaces, and so these discharges are frequently used in electrophotographic (EP) printing processes.[10–17] For example, corona discharges in air are used to sensitize the surface of the photoconductor (PC) in EP printing by electrically charging the surface to an optimum potential.[12–17] Although corona discharges sustained in the air for surface charging do have challenges (e.g., high voltage source and long term deterioration of the PC), the simplicity, high charging efficiency, and low cost of corona charging devices have motivated continued research into optimizing their performance.

The polarity of the corona discharges used for surface charging of PCs depends on the characteristics of the underlying photoconductive coating and toner particles. For example, amorphous selenium coatings perform better when they are charged positively, whereas zinc oxide-resign coatings require negative charging.[13,16,17] Although there are some variations among coatings, negative coronas are most often used for surface charging of PCs. In a typical negative corona discharge, one or more thin metal wires or straight metal blade electrodes are negatively biased to a few hundred volts of dc plus a few kV of ac voltage.[10,11,15] The wires are separated from the PC by gaps ranging from hundreds of

[a)]junchwan@umich.edu
[b)]dhzhang@tju.edu.cn
[c)]napoleon.j.leoni@hp.com
[d)]henryk.birecki@hp.com
[e)]omer_gila@hp.com
[f)]Author to whom correspondence should be addressed. Electronic mail: mjkush@umich.edu.

microns to a few centimeters. The underlying dielectric PC layer is in contact with the ground plane. A large electric field is produced around the wire or tip of the blade by geometric enhancement, and the discharge is initialized when free electrons are accelerated by these strong electric fields to trigger an avalanche.[17,18] This process in negative coronas is particularly sensitive to surface roughness and defects in the electrode that produce additional electric field enhancement or electric field emission of electrons. In negative coronas, the net drift of electrons and negative ions is towards the underlying PC surface, which charges the capacitance of the surface which in turn reduces the electric field in the gap. The surface charging terminates the discharge as long as the discharge is only sustained by a dc (or quasi-dc in a pulsed mode) voltage. The PC charging process functionally operates as a dielectric barrier discharge (DBD).

Corona discharges are used in at least two of the process steps of EP printing—the charging and transfer steps.[13–16] In the charging step, the PC surface is uniformly charged using a corona discharge produced by a corotron or scorotron. The corotron consists of parallel corona wires situated above the PC plate and below a biased electrode. A scorotron is similar to a corotron with the addition of a grid of parallel wires between the corona wires and the PC surface. After the PC surface is charged and the light-induced latent image is formed on this surface, charged toner particles electrically adhere to the latent image. Another corona device is then used to charge the back of the paper to optimize adhesion of toner particles during the transfer of particles from the PC to the paper. In both of these process steps, the underlying dielectric surface moves with speeds of hundreds of cm/s during their charging process with residence times of hundreds of microseconds underneath the corona wire The discharge itself may last for only hundreds of ns. As a result, a non-uniform charge patterns may result due to the interaction between the corona discharge and the moving surface.

In this paper, we discuss results from a computational investigation of a dc blade corona discharge sustained in atmospheric pressure dry air, charging both stationary and moving dielectric surfaces in a DBD configuration, as shown in Fig. 1. For the voltages investigated, we found that the corona discharge is initially sustained by electron impact ionization in the bulk plasma and by secondary electron emission from the cathode. When the underlying dielectric surface charges and voltage is removed from the gap, the electron impact sources from the bulk plasma diminish and the plasma is then sustained by ionization by sheath accelerated secondary electrons from the electrode. Eventually, the plasma extinguishes by charging of the surface in a DBD-like manner. When the dielectric surface moves, the previously charged surface translates away from the corona electrode and is replaced by uncharged surface. This results in an increase in voltage drop across the gap between the corona electrode and the approaching uncharged surface on only one side of the electrode. This rebound in voltage across the gap results in a re-ignition of the discharge. The charging uniformity is sensitive to the material properties of the dielectric sheet, and the subsequent re-ignition of the discharge is sensitive to the previous charging cycle. An oscillatory charging pattern is predicted.

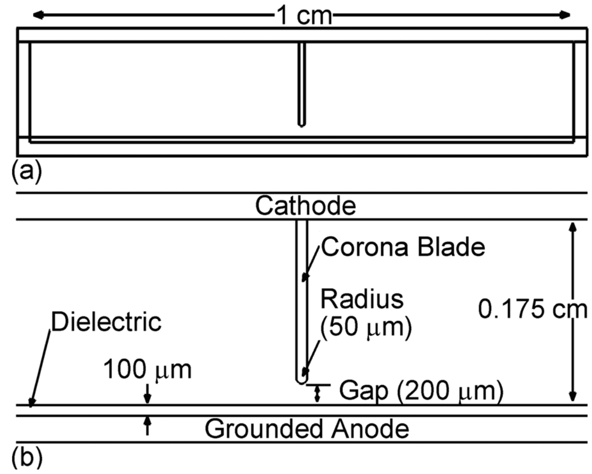

FIG. 1. Schematic of a negatively dc-biased blade corona. (a) Entire device and full computational domain. (b) Enlargement of corona electrode and underlying ground electrode covered with a dielectric PC.

The model used in this investigation is described in Sec. II and followed by a discussion of plasma dynamics of corona and surface charging on a stationary surface in Sec. III. The characteristics of charging of a moving surface are discussed in Sec. IV followed by our concluding remarks in Sec. V.

II. DESCRIPTION OF THE MODEL

The model used in this investigation, *nonPDPSIM*, is described in detail in Refs. 19 and 20. Briefly, *nonPDPSIM* is a two-dimensional, multi-fluid hydrodynamics simulation. Continuity equations for the density of electrons and ions, for charge on surfaces and within conductive materials, and Poisson's equation for electric potential are simultaneously integrated using a fully implicit Newton-Raphson iterative scheme. The fluxes of charged particles are given by the Scharfetter-Gummel discretization technique[21] with numerically derived Jacobian elements. The divergence operators are couched in finite volume form, which is fully conservative. The timesteps enabled by this implicit technique can exceed the Courant-Friedrichs-Levy (CFL) and dielectric relaxation time constraints. Poisson's equation is solved in the entire computational domain except for metals where the potential is specified as a boundary condition. On non-metal points on the boundaries of the computational mesh, von Neumann conditions are imposed. All surfaces are absorbing for charged particles incident onto the surface with neutral counterparts returning to the plasma and secondary electrons emitted for positive ions and photons as discussed below. The incoming and outgoing charged particle fluxes are then used as sources for surface charge.

A single integration timestep for the charged particles and potential is followed by an implicit integration of the continuity equations for neutral particles, in this case including only diffusive transport. Finally, the electron energy transport equation is implicitly integrated for the bulk electron temperature. Rate coefficients and transport coefficients for bulk electrons are obtained from local solutions of Boltzmann's equation for the electron energy distribution (EED), which are interpolated from a table on the basis of local electron temperature. This table is updated every 0.1 ns during the simulation to account for the change in species mole fractions. The differential equations are discretized using finite volume techniques, and the numerical grid uses a boundary fitting unstructured mesh with triangular elements with multiple refinement zones. Once the electric potential, charge density, and electron temperature have been updated, radiation transport is addressed using a Greens function approach. ultra-violet and vacuum ultraviolet (UV/VUV) radiation is produced by relaxation of high-lying excited states of N_2.

An electron Monte Carlo simulation (eMCS) is used to track the trajectories of secondary electrons emitted from all surfaces. EEDs are separately computed for the secondary electrons, which are then used to produce excitation and ionization sources. In the eMCS, a spatially fine Cartesian mesh is overlaid onto the unstructured mesh. Electron trajectories are computed on the Cartesian mesh enable more efficient algorithms. Electron impact source functions are computed and then interpolated between the structured and unstructured mesh. Sources of secondary electrons from surfaces include those produced by ion and photon fluxes. The secondary emission coefficients used in this investigation were 0.15 and 0.1 for all the positive ions and photons, respectively.

To enable an investigation of plasma-surface interactions during charging with moving surfaces, an idealized corona device has been modeled, as shown in Fig. 1. The device consists of a top cathode and a metal wire corona (or a metal corona blade) biased with negative dc voltage up to 4.5 kV. The metal blade has a thickness of 100 μm and a height of a 1.55 mm. The radius of curvature of the blade tip is 50 μm. An underlying dielectric sheet (100 μm thick and $\varepsilon_r = \varepsilon/\varepsilon_0 = 5$) is separated from the corona tip by a 200 μm gap in the base case. This dielectric target (intended to represent paper or a photoconductor layer in EP printing) serves as a perfect insulator (the conductivity is zero), so the surface charges are laterally immobile on the dielectric sheet. The dielectric target is in contact with the grounded anode and is initially uncharged. The mesh consists of about 12 800 computational nodes of which about 9000 nodes are in the plasma zone. The finest mesh spacing is 9 μm in the gap between the corona tip and dielectric sheet. The lateral side dielectric boundaries in the simulation are placed far from the corona wire so that the potential calculation will not be affected. Although corona wires are typically used in arrays in EP applications, we investigated a single corona source using Cartesian geometry to study possibly asymmetric plasma-surface interactions on stationary and moving surfaces.

The moving surface was computationally addressed in the following manner. The numerical mesh points on top of the surface in contact with the plasma are chosen to be evenly spaced. These mesh points are identified during code initialization and sifted into an array based on horizontal position. The surface is moved every $\Delta t = \Delta x / v$ s, where Δx is the mesh spacing on the surface and v is the horizontal speed of the surface. Assuming that the surface is moving right-to-left, motion of the surface consists of translating the properties of the mesh point (e.g., chemical composition and surface charge density) one location to the left. The properties of the leftmost mesh point are translated out of the computational domain and no longer affect the simulation. The properties of the rightmost mesh point are set to the initial or prescribed conditions, which in this case is a zero surface charge density.

The gas is 1 atm of dry air and the gas temperature is held constant at 300 K. Due to the magnitude of the calculation, we use a reduced reaction mechanism containing a subset of the reactions described in Refs. 22 and 23 to minimize the computation time. The reduced reaction mechanism includes N_2, $N_2(v)$, N_2^{*}, N_2^{**}, N_2^{***}, N_2^{+}, N_4^{+}, N, N^{*}, N^{+}, O_2, $O_2(^1\Delta)$, O_2^{+}, O_2^{-}, O_3, O^{-}, O, $O(^1D)$, O^{+}, and electrons. The states N_2^{*} and N_2^{**} are nominally N_2(A,B) and N_2(C), though the latter is treated as a lumped state including transitions higher than N_2(C). N_2^{***} is nominally $N_2(a')$ though it is also a lumped state accounting for higher levels. The discharge is initiated by placing an electrically neutral electron-ion cloud with a peak density of $10^{12}\,\mathrm{cm}^{-3}$ and radius of 200 μm around the corona tip. The timestep is typically 5×10^{-12} s.

III. CORONA PROPERTIES AND CHARGING OF A STATIONARY SURFACE

The characteristics of the blade corona discharge and charging of the underlying stationary dielectric surface will first be discussed. The corona was first biased to -3 kV and the dielectric constant of the underlying insulating sheet in contact with ground was $\varepsilon_r = 5$. The time evolution of the electron density and electric potential during the surface charging process is shown in Fig. 2. The electron impact ionization sources by bulk electrons S_e and beam-like secondary electrons S_{sec} are shown in Fig. 3. Due to the high gap-averaged electric field of 136 kV/cm (E/N ≈ 556 Td, 1 Td = $10^{-17}\,\mathrm{V\,cm}^2$) between the corona tip and dielectric surface and the geometrically enhanced electric field at the corona tip, an electron avalanche occurs within a few ns. Ionization is provided by lower energy bulk electrons and by electrons emitted from the cathode blade through ion and photon secondary emission and accelerated by the large sheath potential. Before the dielectric is charged and while the full applied potential is dropped across the gap (0.1 ns in Fig. 3), the rate of ionization directly underneath the blade corona by bulk electrons, 10^{23}–$10^{24}\,\mathrm{cm}^{-3}\,\mathrm{s}^{-1}$, dominates. Ionization from secondary electrons is generally 2 orders of magnitude smaller due to the small ion flux at this time producing a low rate of secondary emission, and the lack of a fully formed sheath at the cathode. Electrons drifting towards the underlying dielectric sheet negatively charge the surface. As the plasma channel becomes conductive and the dielectric charges, the electric potential is shielded by the bulk plasma, while electric potential lines are trapped in the dielectric due to the surface charging. At t = 2 ns, plasma densities of up to $10^{15}\,\mathrm{cm}^{-3}$ are generated at the corona tip which fully form the sheath. The electron density at mid-gap is on the order of $2 \times 10^{13}\,\mathrm{cm}^{-3}$.

As the discharge proceeds, the charging of the lower surface reduces the voltage drop and E/N between the corona

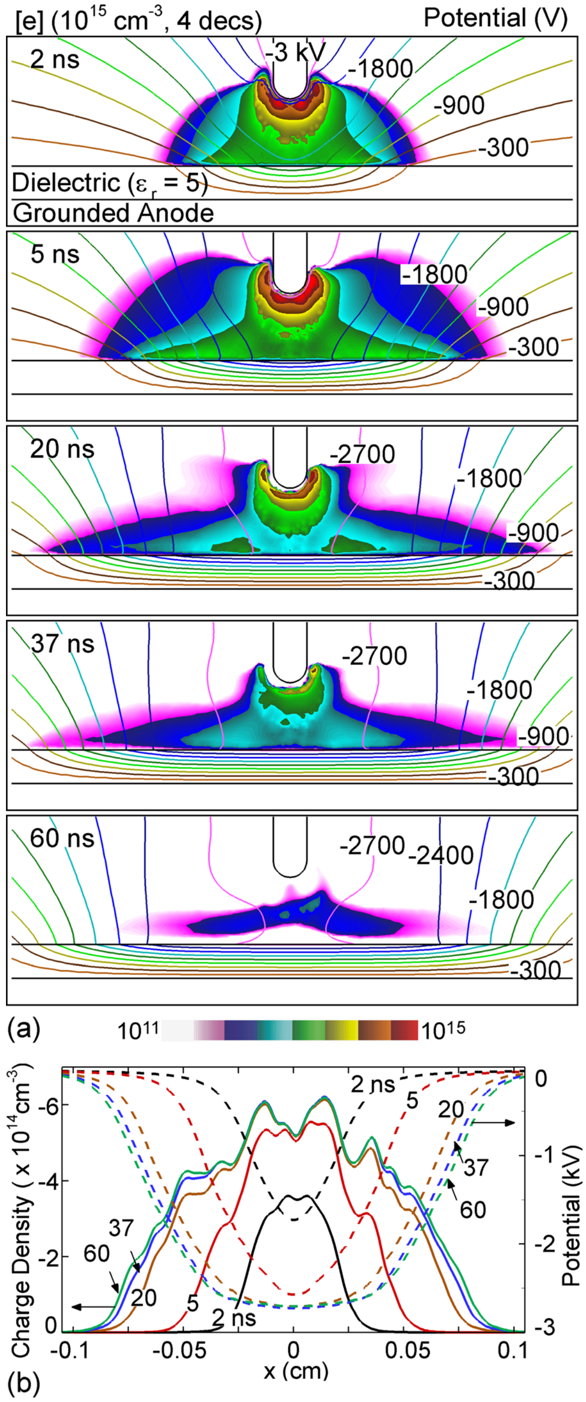

FIG. 2. Charging of PC surface by a -3 kV dc biased corona blade. (a) Time evolution of electron density (color flood, cm^{-3}) and electric potential (contour lines, V). (b) Time evolution of surface charge density (solid, cm^{-3}) and surface voltage (dashed, V) on the PC. The discharge is terminated by surface charging. The electron density is plotted on a log-scale over 4 decades (10^{11}–10^{15} cm^{-3}).

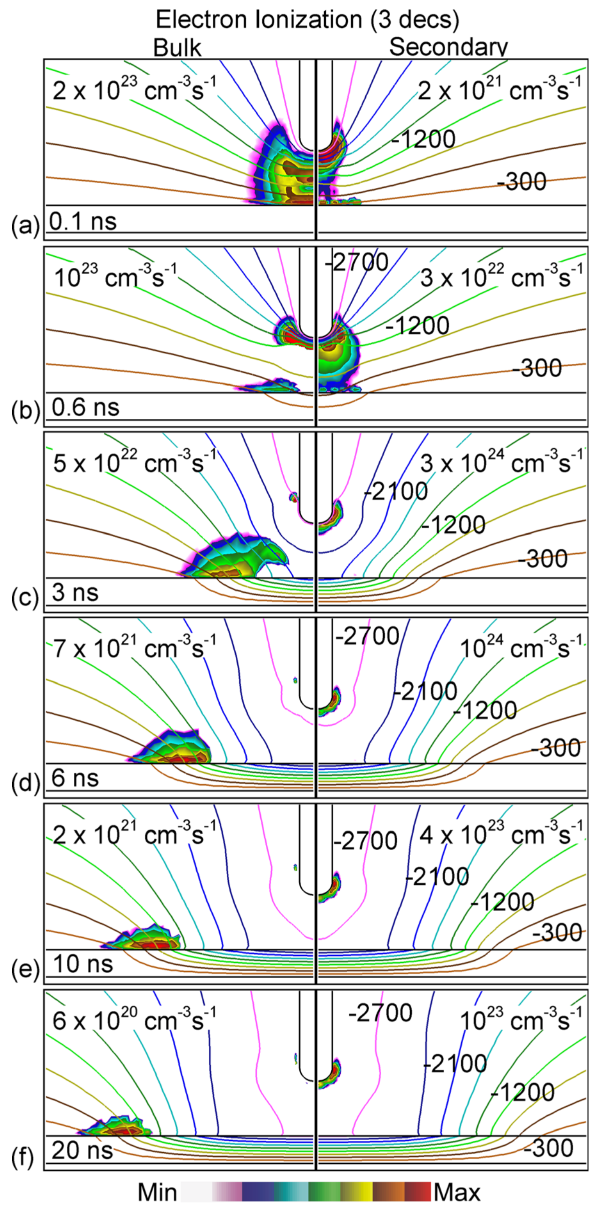

FIG. 3. Electric potential (contour lines) and electron impact ionization sources (color flood, cm^{-3} s^{-1}) by bulk electrons (S_e) and by sheath accelerated secondary electrons (S_{sec}) at different times after initiation of the discharge. The charging of the surface far from electrode results from a surface ionization wave. The ionization sources are plotted on a log scale over 3 decades with the maximum value noted in each frame.

blade and the dielectric and so decreases the rate of electron impact ionization from bulk plasma electrons in the gap beneath the tip. However, electron impact ionization from sheath accelerated secondary electrons still occurs due to UV photon and positive ion bombardment of the negatively biased corona blade. At t = 3 ns, this ionization source at the tip, S_{sec}, is up to 3×10^{24} cm^{-3} s^{-1}. At this stage, the corona discharge is primarily sustained by secondary electron ionization processes.

The voltage drop in the gap directly underneath the corona tip is reduced by charging of the capacitance of the PC. However, there is still a large potential drop between the corona blade and the uncharged surface of the PC to the left and right of the centrally charged PC surface. The conductive plasma in the gap results in the majority of the voltage between the corona tip and the uncharged dielectric being dropped across the edge of the plasma and the uncharged PC surface. The result is a surface ionization wave (SIW) at the edge of the plasma, which propagates laterally outwards with a speed of 5×10^6 cm s^{-1}. The E/N at the surface in the SIW is 330 Td, which supports an ionization rate of 9×10^{21} cm^{-3} s^{-1}. As the SIW propagates, the underlying PC is charged. The spreading of the discharge on the surface is symmetric as there is uncharged dielectric on both sides of the blade and this produces SIWs propagating in both directions. By 60 ns, the SIWs dissipate as the finite voltage drop in the plasma (and distance from the corona blade) reduces the E/N in the SIW below the self-sustaining value. At this time, the dielectric surface underneath the corona blade is fully charged to a distance of 0.1 cm on either side of the blade. This charging process is similar to those occurring in conventional DBDs.[24–27]

The time evolution of the surface charge density and electric potential on the PC surface is shown in Fig. 2(b). (The surface charge densities are slightly smoothed to reduce the noise in the charging due to the randomness of the Monte Carlo simulation used for secondary electrons.) The PC surface is rapidly charged during the first 20 ns. The charging during the first 5 ns is directly under the corona blade by ionization in the bulk plasma above the PC. After the first 5 ns, charging is primarily due to the propagation of the oppositely directed SIWs. Charging largely terminates by about 40 ns and the SIWs have completely dissipated by 60 ns. At this time, the average electron density in the gap decreases to $10^{11}\,\mathrm{cm}^{-3}$, and the discharge terminates. The peak voltage on the PC surface underneath the corona tip after the termination of the discharge is -2.7 kV for an initial corona bias voltage of -3.0 kV.

Strictly speaking, conventional negative corona discharges are sustained by the high electric field near the surface of a small radius-of-curvature electrode due to geometrical field enhancement.[28,29] This geometrical field enhancement decreases with distance from the tip of the corona blade (or wire) and local ionization rates scale exponentially with the local electric field. At a critical distance from the tip, the electric field is sufficiently small that electron impact ionization is reduced below self-sustaining. At that point in an attaching gas such as air, the electrons are consumed by formation of negative ions, and current continuity is then carried by drift of the negative ions.[28–31]

In this particular geometry and in most EP applications of corona, the PC surface is still within the high electric field region, and so the transition to a classical corona discharge where current is dominantly carried by negative ions does not occur. The proximity of the ionization by sheath phenomena is therefore important. For example, the electron density and electric potential with and without ionization by sheath accelerated secondary electrons, S_{sec}, are shown in Fig. 4(a). At t = 30 ns before the discharge terminates, S_{sec} provides an ionization source of $5.8\times10^{22}\,\mathrm{cm}^{-3}\,\mathrm{s}^{-1}$ with an electron density up to $2.4\times10^{14}\,\mathrm{cm}^{-3}$ in the gap, which helps to maintain the discharge while charging the underlying dielectric more negatively. The peak electron density in the gap reduces to $10^{11}\,\mathrm{cm}^{-3}$ within 87 ns. Without $\mathrm{S_{sec}}$, the discharge is terminated earlier as the peak electron density reduces to $10^{11}\,\mathrm{cm}^{-3}$ within 56 ns. The surface charge density and potential on the PC after the discharge has been terminated for both cases are shown in Fig. 4(b). With S_{sec}, the surface potential reaches -2.7 kV and charging extends to ±1 mm. Without S_{sec}, the surface potential reaches only -2.2 kV and charging extends only to ±0.75 mm. The ionization resulting from secondary electron emission enables the discharge to be sustained for a longer time and so more

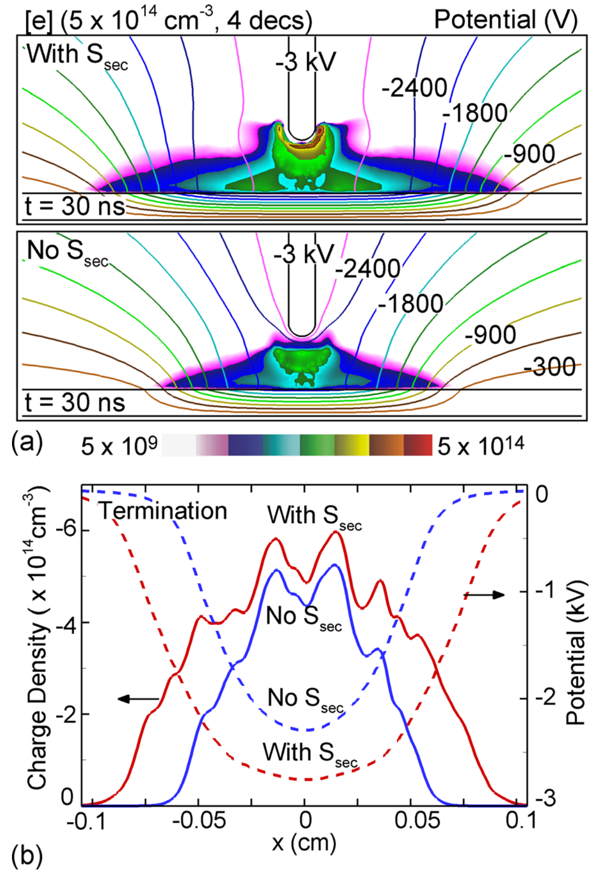

FIG. 4. Ionization by secondary electrons S_{sec} helps to maintain the corona discharge. (a) Electron density (color flood, cm^{-3}) and electric potential (contour lines, V) produced by a -3 kV dc biased wire corona at t = 30 ns with and without ionization sources by sheath accelerated secondary electrons (S_{sec}). (b) Surface charge density (solid, cm^{-3}) and surface voltage (dashed, V) with and without S_{sec} showing the contribution of secondary electrons. The electron density is plotted on a log-scale over 4 decades (5×10^{10}–$5\times10^{14}\,\mathrm{cm}^{-3}$).

fully charge the PC. Without S_{sec}, the discharge terminates at about 40 ns and with S_{sec}, the discharge terminates at 60 ns.

Although the PC surface is close to the corona tip and current continuity is provided primarily by drift of electrons in geometry, negative ions are still formed during the charging process– O^- through dissociative attachment to O_2 and direct attachment to form ${O_2}^-$. The time evolution of electron density, total negative ion density, electric potential, surface charge density, and potential on PC surface is shown in Fig. 5. The sequence begins at 50 ns when the discharge has nearly terminated due to surface charging and the reduction in voltage across the gap. The low electron temperature in the gap, 0.5 eV, is well below the self-sustaining value of about 2.5 eV and so attachment to O_2 dominates. At 50 ns, the electron density of $7\times10^{12}\,\mathrm{cm}^{-3}$ begins to decay through recombination, attachment, and drift onto the PC surface. At this time, the peak negative ion density is $1.6\times10^{13}\,\mathrm{cm}^{-3}$ near the corona tip. By 200 ns, the electron density has decayed to $3\times10^{9}\,\mathrm{cm}^{-3}$ while the negative and positive ion density is $3\times10^{12}\,\mathrm{cm}^{-3}$. At this time, the recombining plasma consists mostly of negative and positive ions. This plasma then slowly decays dominantly by ion-ion recombination over a period of up to 1 μs. The surface

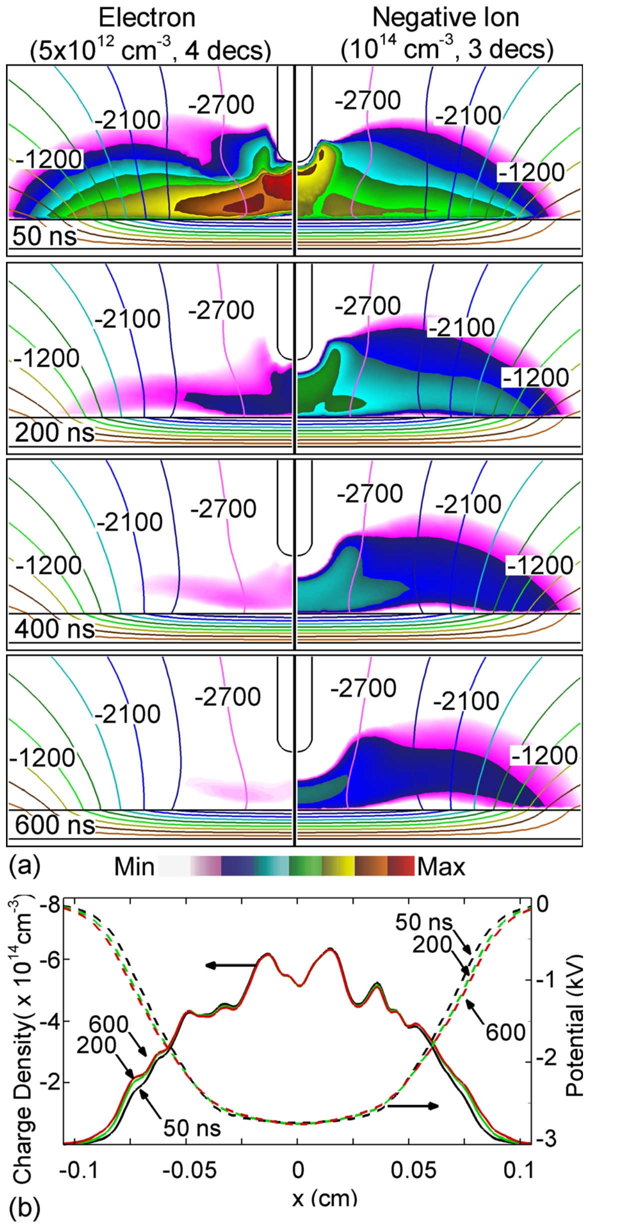

FIG. 5. Residual electrons and negative ions produce nominal charging of the PC after the discharge is terminated. (a) Time evolution of electron and negative ion density (color flood, cm^{-3}) and electric potential (contour lines, V) at t = 50, 200, 400, and 600 ns. (b) Time evolution of surface charge density (solid lines, cm^{-3}) and surface voltage (dashed lines, V) at t = 50, 200, and 600 ns. The electron density is plotted on a log-scale over 4 decades, and the negative ions are plotted over 3 decades. The maximum value is noted in each frame.

charge density and surface potential change very little from 50 ns to later times in spite of the large remaining ion density. First, the electric field in the gap is small (7 kV/cm, $E/N \approx 30$ Td at t = 200 ns) and so there is little drift of ions to the surface. Second, the drift of ions to the surface is largely ambipolar. That is, the negative and positive ions drift at the same rate. As a result, there is not a net current to the surface to further charge the PC.

During the active discharge, the peak value of volumetric photoionization source S_{ph} is on the order of $10^{19}\,cm^{-3}\,s^{-1}$, which is small compared to electron impact ionization sources. Having said that, this photoionization source and photoemission produced by UV photons from long-lived excited states continuously provide seed secondary electrons at the dielectric and electrode surfaces. Subsequent avalanche by these secondary electrons then helps to maintain the discharge through either sheath accelerated secondary electrons at the cathode or by helping to maintain the SIW. For example, the electron density and electric potential with and without volumetric photoionization and photoemission from the corona wire and PC surface during surface charging (at t = 30 ns) are shown in Fig. 6. The surface charge density and potential on the PC after the discharge is terminated are also shown in Fig. 6. Although the contribution of S_{ph} is small and the change in peak electron density is small, the plasma density is more spatially uniform when including the photoionization. Due to the somewhat lower impedance of the discharge due to photoemission at the cathode surface, the final potential and surface charge density with S_{ph} are nominally higher than for discharges without S_{ph}.

After initiation of the discharge, the applied voltage is divided between the sheath at the electrode, the plasma column, the avalanche front, the surface sheath capacitance after the discharge strikes the surface, and the capacitance of the PC as the surface charges. For a given surface charge, the voltage drop in the dielectric ΔV_d is inversely proportional to the capacitance (per unit area) of the PC, $\varepsilon_r\varepsilon_0/d$. By

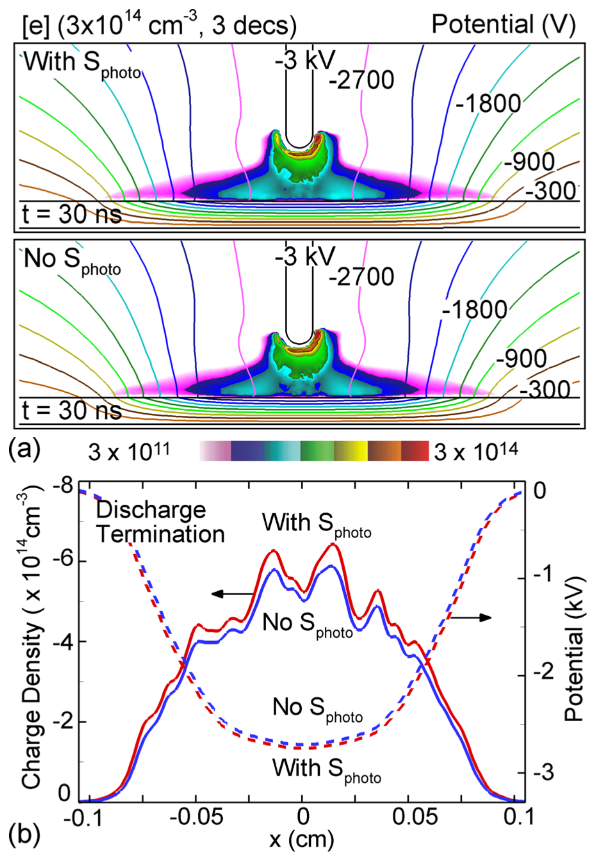

FIG. 6. Plasma properties produced by a −3 kV dc biased corona blade at t = 30 ns with and without volumetric photoionization source S_{ph} and photoemission from the blade and PC surface. (a) Electron density (color flood, cm^{-3}) and electric potential (contour lines, V). (b) Surface charge density (solid lines, cm^{-3}) and surface voltage (dashed lines, V). The electron density is plotted on a log-scale over 3 decades (3×10^{11}–$3 \times 10^{14}\,cm^{-3}$).

controlling the capacitance of the PC, the sheath voltage, electron impact ionization rates, and so spreading of the plasma along the surface can be controlled and optimized. For example, the electron density and electric potential at t = 60 ns before the discharge terminates, and the surface charge density and potential on PC surface after the termination of discharge are shown in Fig. 7 for PCs having $\varepsilon_r = 5$, 10, and 20. At termination of the discharge, the voltage drop in the dielectric is 310, 170, and 100 V for $\varepsilon_r = 5$, 10, and 20. For the PC having a large capacitance, the voltage across the gap remains large for a longer period of time since the higher capacitance of the PC requires a longer time to charge. As a result, the discharge for $\varepsilon_r = 5$ at t = 60 ns has a smaller electron density and begins to terminate earlier than the discharge on a PC surface with $\varepsilon_r = 20$. At this time, the maximum electron density at mid-gap is $5.9 \times 10^{12}\,\mathrm{cm}^{-3}$ for $\varepsilon_r = 20$ compared to $5 \times 10^{11}\,\mathrm{cm}^{-3}$ for $\varepsilon_r = 5$. Since the terminal electrical potential of the surface after charging is approximately the same for all ε_r, the maximum surface charge is then in proportion to ε_r. The larger capacitance requiring more current to charge the PC results in a longer discharge pulse (a longer *RC* time constant) and produces a higher electron density. However, the spatial extent of the surface charge is a weak function of ε_r. The SIW that laterally extends charge on the surface is driven, in part, by the horizontal component of the electric field at the surface of the PC. Although the surface charge is larger with larger ε_r, the surface potential is nearly the same. As a result, the horizontal component of the electric field that drives the SIW is a weak function of ε_r.

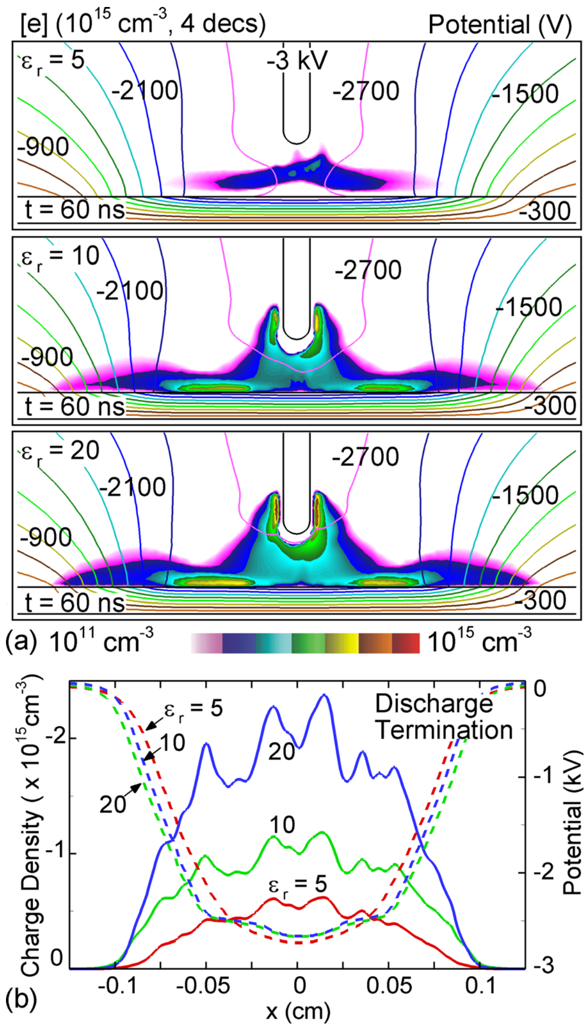

FIG. 7. Plasma properties produced by a −3 kV dc biased corona blade at t = 60 ns for the PC having relative permittivities ε_r of 5, 10, and 20. (a) Electron density (color flood, cm^{-3}) and electric potential (contour lines, V). (b) Surface charge density (solid lines, cm^{-3}) and surface voltage (dashed lines, V) on PC surface after termination of the discharge. The electron density is plotted on a log-scale over 4 decades (10^{11}–$10^{15}\,\mathrm{cm}^{-3}$).

IV. CHARGING OF A MOVING SURFACE

When a corona discharge is used for continuous surface charging, the underlying dielectric is in motion during the charging process. For a stationary uncharged target, the charging process by a dc (or quasi-dc) corona discharge behaves like a DBD. The charging of the surface is symmetric on either side of the corona tip. Surface charging reduces the electric field in the gap which then terminates the discharge. In the case of a moving surface, as the dielectric surface underlying the discharge moves, surface charge is translated away from the corona electrode on one side, while uncharged dielectric translates towards the corona electrode on the other side. As a result, the incoming uncharged (or partially charged) surface restores the voltage drop in the gap that had previously been reduced by surface charging. This restoration of voltage may then re-ignite the plasma, which then charges the fresh incoming surface.

At atmospheric pressure, the plasma formation and decay times can be as short as tens of ns, whereas the residence time of the moving charged surface before the plasma is reignited may be a few hundred microseconds. The surface moves in an almost quasi-static fashion which is much slower than the spreading of the plasma. As a result, it is difficult to address the surface moving at its actual speed in the model while also simulating plasma processes having sub-ns timescales with many to tens of ps timesteps. Given that the plasma does terminate due to surface charging, it may not be necessary to address the entire time while the surface charge is moving after the discharge terminates and before it reignites. To address the continuous motion of the PC, the following technique was used in the first cases investigated.

The PC surface was assumed to enter from the right and exit to the left in Fig. 8. The plasma is first simulated until charging of the dielectric terminates the discharge, producing a symmetric charging pattern. This surface charge density is then translated to the left in 100 μm increments, which brings in uncharged PC from the right while extending the region of charged surface to the left. This results in an asymmetric electrical potential distribution, as shown in Fig. 8(a). This asymmetric potential compresses contours of electric potential into the cathode and produces a progressively larger electric field at the corona electrode on the side of the electrode facing the incoming charged surface. The translation of the surface continues until the electric field is large enough to re-ignite the plasma, which occurs here for a shift of the surface to the left of 500 μm. This re-ignition process, illustrated by the time evolution of electron density, electric potential,

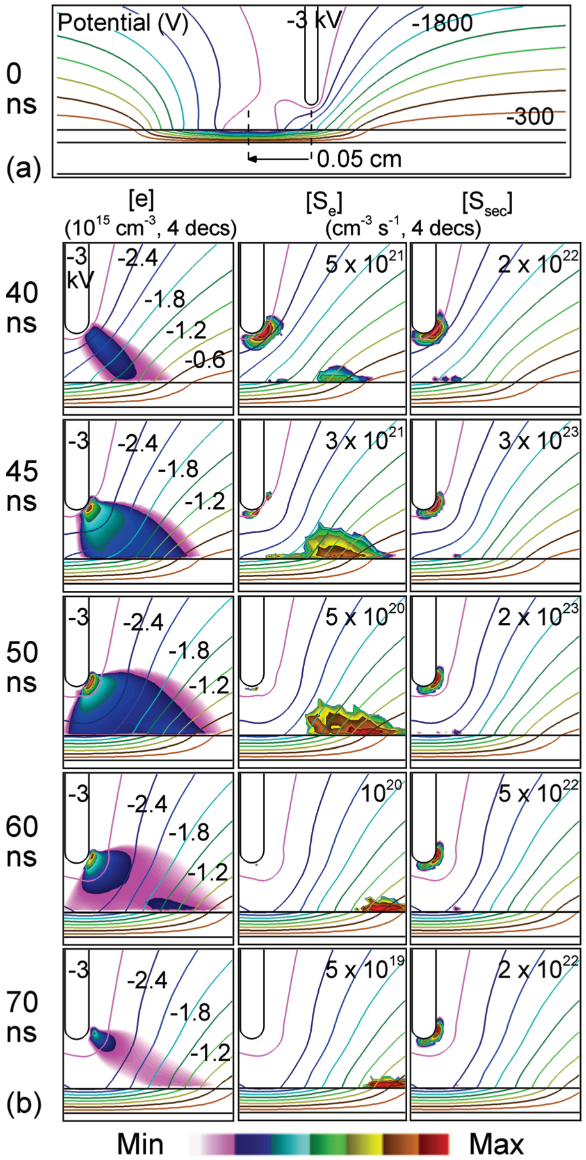

FIG. 8. Time evolution of electron density (flood, cm^{-3}), ionization sources from bulk electrons S_e, ionization by secondary electrons S_{sec} (flood, cm^{-3} s^{-1}), and electric potential (contour lines, V) produced during reignition after the first symmetric surface charge density was shifted to the left by 500 μm. Values are plotted on a log-scale over 4 decades with the maximum value noted in each frame.

and ionization sources from bulk and secondary electrons, is shown in Fig. 8(b). This sequence is for the second discharge which follows translation of the first symmetrically charged surface to the left. Time t = 0 corresponds to when the second discharge re-ignites, approximately the time shown in Fig. 8(a). At t = 40 ns, ionization for the second discharge is dominated by sheath processes (both bulk and secondary emission) at or near the cathode and by restarting of the SIW. The ionization sources are 10^{21}–10^{22} cm^{-3} s^{-1}. The electron source in the bulk plasma is generally comparable with the source from secondary electron ionization at the corona tip.

The reignited discharge is asymmetric, with plasma preferentially produced on the side of the corona electrode facing the uncharged dielectric where the voltage drop across the gap is the largest. Note that at the time of re-ignition, there is a small secondary electron ionization source at the surface of the PC. These secondary electrons are produced largely by photo-electron emission at a time that the charging of the surface produces a larger horizontal component of the electric field than a vertical component, which would otherwise accelerate the secondary electrons back into the surface. These secondary electrons are then accelerated parallel to the surface for about 100–200 μm prior to impacting the PC. A small ionization source then results.

At t = 50 ns, the second discharge is fully developed. The plasma density is generally smaller (10^{12} cm^{-3} at mid-gap) compared to the first discharge pulse (10^{13} cm^{-3} at mid-gap) as the bulk electric field is smaller for at least two reasons. First, re-ignition occurs when the voltage drop across the gap is less than the initial charging voltage due to the prior charging of the dielectric. Second, the effective gap length for the first pulse is the geometrical vertical distance between the tip of the corona bar and the surface of the PC, 200 μm, which produces a gap-averaged E/N = 556 Td. For re-ignition, the effective gap length is along the electric field line originating on the cathode at the site of the maximum electric field and ending on the uncharged surface entering from the right. This distance is 300 μm at re-ignition, producing a gap averaged E/N = 270 Td. After the second discharge pulse fully develops, the conductive plasma at the side of the corona tip shields the electric field and diminishes the electron source in the bulk plasma. The re-ignition is then dominated by the secondary electron ionization source, S_{sec}. As the SIW charges one side of the surface and reduces the electric field in the gap, the second discharge pulse then starts to extinguish. This general sequence of events is repeated as fresh, and uncharged PC surface is translated towards the corona electrode from the right.

The total surface charge density and surface potential on the PC surface before and after re-ignition of a secondary discharge are shown in Fig. 9, while initial surface charge density is shifted up to 700 μm. The total surface charge density and surface potential on the dielectric after 5 discharge pulses (4 re-ignitions) are shown in Fig. 10. In general, the discharge cannot be reignited until the surface is translated to the left by at least 300–500 μm, which results in a rebound of gap voltage up to 1.1 kV. With each successive re-ignition, the surface is incrementally charged over another 100–200 μm. The maximum surface charge incrementally produced with each re-ignition is about the same compared to the initial pulse, with perhaps a small increase. Although there is a bit of statistical noise in the charging, there is also an oscillatory maximum in the surface charge density and potential. In a continuous charging process, the following basic sequence is repeated: ignition, surface charging, SIW, discharge termination, motion of the surface, restoration of gap voltage, and re-ignition. The requirement for re-ignition is to have a critically large E/N, which produces a rapid avalanche which in turn charges the surface. The resulting SIW extends the charging beyond the point that the surface must reach to create the critical E/N. This process of re-ignition and SIW naturally produces an oscillatory charging pattern.

The pattern of the surface potential and its peak value are expected to be sensitive to the design of corona device

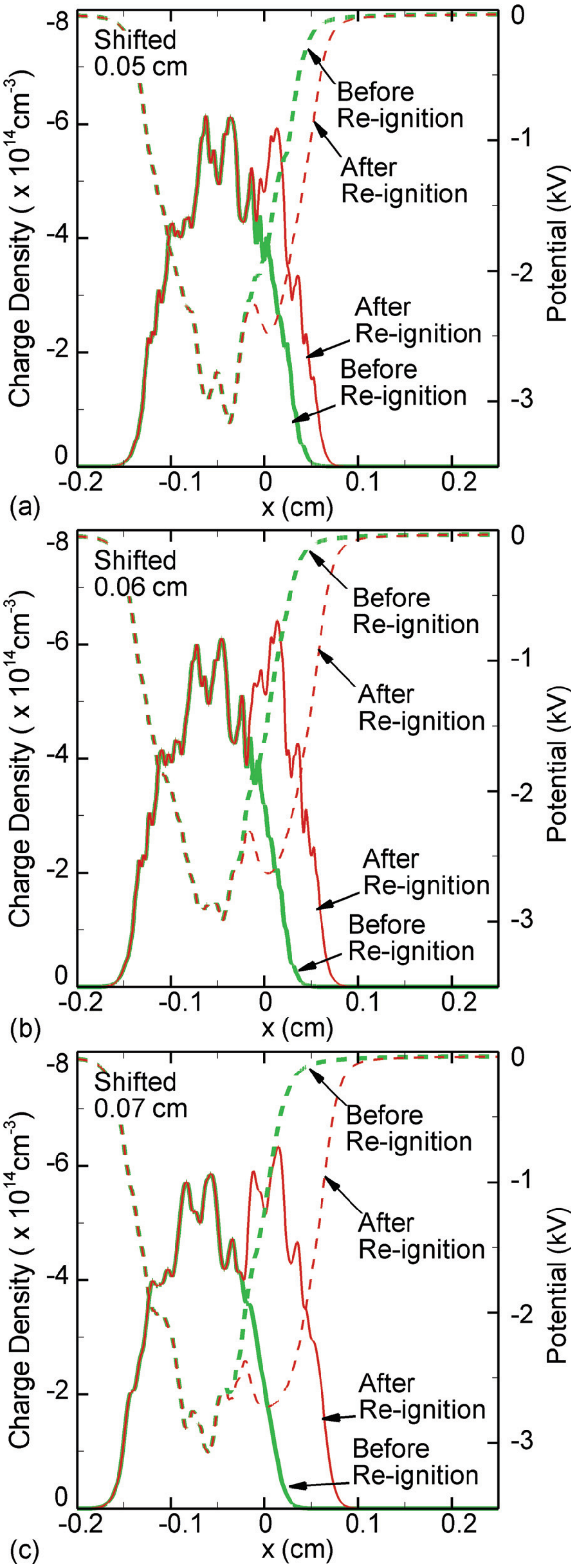

FIG. 9. The total surface charge density (solid lines, cm^{-3}) and surface potential (dashed lines, V) before and after re-ignition of the discharge with a shift of initial surface charge density by (a) 500 μm, (b) 600 μm, and (c) 700 μm.

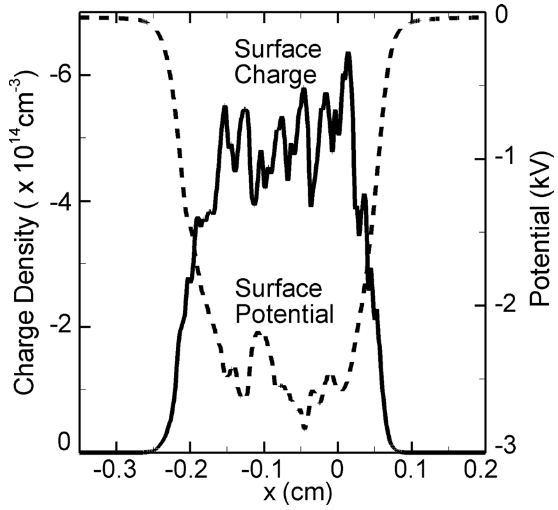

FIG. 10. The total charge density (solid lines, cm^{-3}) and surface potential (dashed lines, V) on the dielectric surface after 5 discharge pulses (4 re-ignitions).

(speed of surface movement, voltage waveform, and dielectric materials), since the re-ignition strongly depends on feedback from the previous surface charging cycle. For purposes of demonstration, the time evolution of electron density and electric potential of a corona discharge onto a continuously fast-moving surface are shown in Fig. 11(a). The corresponding total charge density and electric potential on the moving surface are shown in Fig. 11(b). The blade corona is biased with -3 kV dc and the underlying dielectric moves from right to left at a speed that is commensurate with the spreading of the plasma by the SIW. The moving dielectric continuously translates uncharged fresh surface towards the blade corona. When the voltage drops between the blade corona and uncharged surface rebounds, an electron avalanche occurs, and the corona discharge is then reignited. The charged surface translating to the left terminates the discharge on the left side of the electrode while the corona blade continuously sees the fresh surface underneath the tip as the surface enters from the right. The end result is that the discharge continuously and uniformly charges the underlying dielectric, and the surface charging is asymmetric with respect to the corona electrode but more uniform. The oscillatory charging pattern on the surface results from discrete re-ignition events which in turn result from the rapid charging of the surface and the relatively slow moving surface. A more uniform surface charging might be obtained by using a gas mixture with long lived excited states capable of continuously emitting UV/VUV photons which produce photoemission on a fast moving surface. This photoemission will help to maintain the SIW in a continuous manner.

In addition to controlling the capacitance of PC dielectric, the peak surface potential can also be adjusted by varying the gap distance between corona tip and the underlying surface. The electron density and electric potential during the charging process at t = 20 ns are shown in Fig. 12(a) for varying the applied dc voltage (V_a) and gap size (d_g) while keeping the ratio constant ($V_a/d_g = 15$ kV/mm). V_a varies from -1.5 kV to -4.5 kV for gaps of 100 μm to 300 μm. The surface charge density and surface potential after the discharge has terminated are shown in Fig. 12(b). Although the gap averaged E/N is the same in all cases, the geometrically enhanced electric field significantly increases with increased

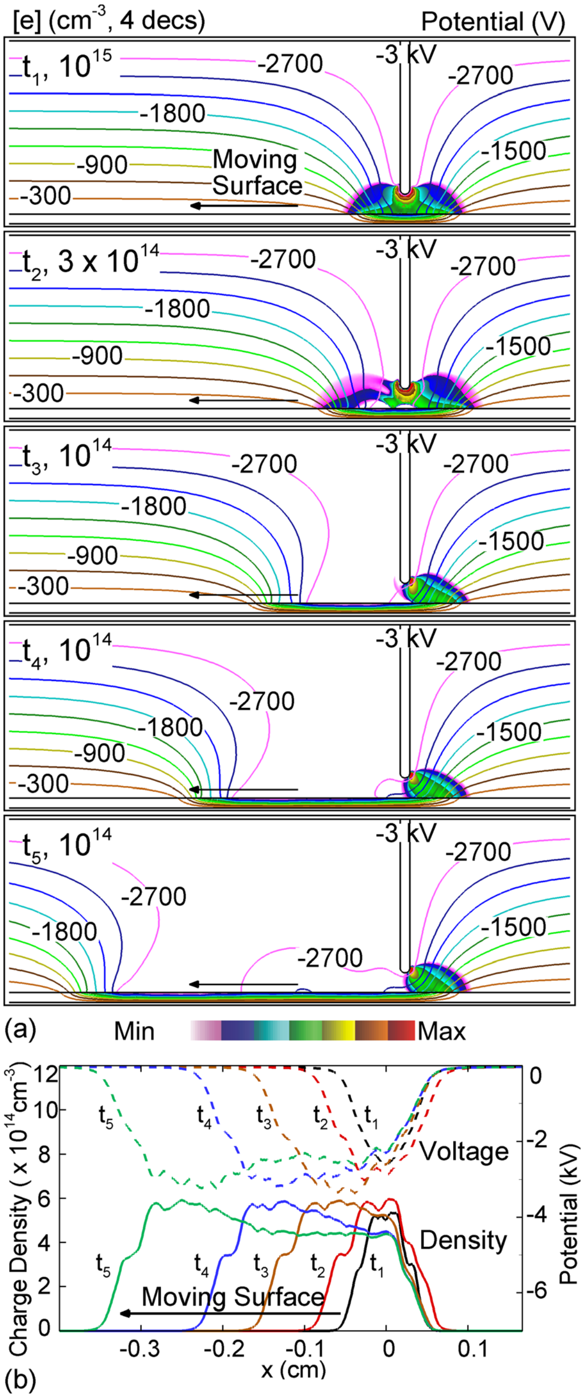

FIG. 11. Time evolution of (a) electron density (flood, cm^{-3}) and electric potential (contour lines, V) and (b) total surface charge density (solid lines, cm^{-3}) and surface potential (dashed lines, V) on a rapidly moving surface. The discharge is continuously re-ignited by the rapidly moving surface in a quasi-dc manner. The electron density is plotted on a log-scale over 4 decades with the maximum value noted in each frame.

dc voltage on the corona tip. As a result, the higher electric field produced at the corona tip biased with -4.5 kV with the larger gap produces a more intense ionization source, a higher electron density, and wider region of surface charging. The larger voltage also requires more current and a longer time to charge the surface of the PC which provides more time for the SIW to propagate to charge more surface. Surface charging with the lower voltage and smaller gap is more confined.

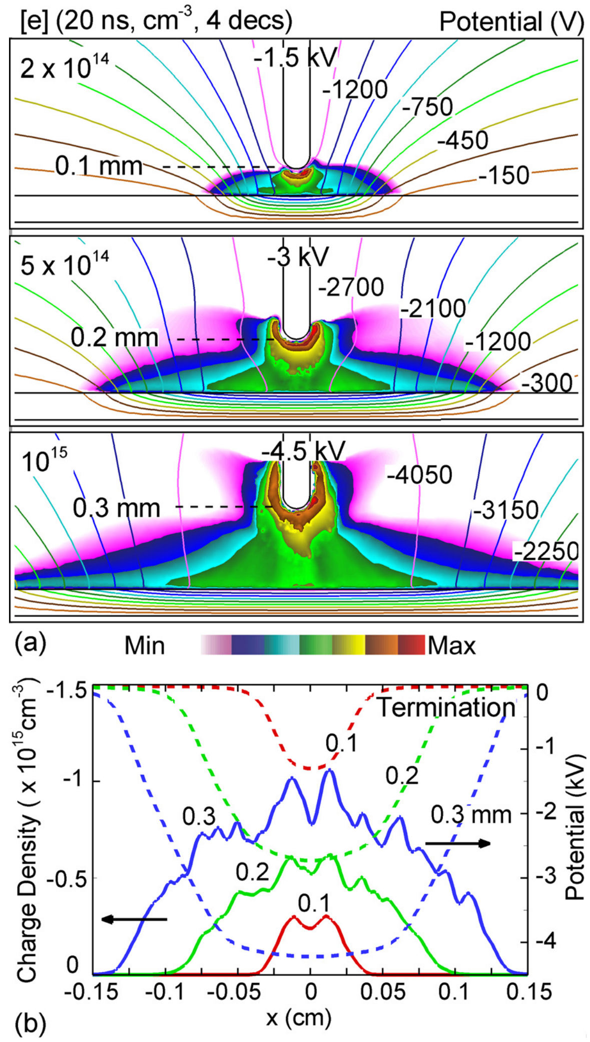

FIG. 12. Time evolution of (a) electron density (flood, cm^{-3}) and electric potential (contour lines, V) during the charging process at t = 20 ns and (b) total surface charge density (solid lines, cm^{-3}) and surface potential (dashed lines, V) after the termination of discharge. Results are shown for V_a/d_g = -1.5 kV/0.1 mm, -3 kV/0.2 mm, and -4.5 kV/0.3 mm, where V_a is the applied dc voltage and d_g is the gap size. The electron density is plotted on a log-scale over 4 decades with the maximum value noted in each frame.

V. CONCLUDING REMARKS

Corona discharges sustained in atmospheric pressure air are important in many EP printing technologies to charge the underlying dielectric PC surfaces. We computationally investigated the behavior of an idealized corona discharge and surface charging when the PC surface is stationary and in motion. We found that electron impact ionization by electrons in the bulk plasma initializes the discharge underneath the corona tip, however, prior to the discharge terminating, ionization is provided dominantly by sheath accelerated secondary electrons. Electrons negatively charge the underlying dielectric, trapping electric potential lines in the dielectric and removing voltage from the gap. The electrons carry the vast majority of current to the dielectric in this particular geometry with little contribution from negative ions. A higher electron density and higher surface charge density can be produced on PCs having higher dielectric constants due to larger voltage across the gap and longer charging time. On a stationary dielectric, a surface ionization wave spreads outwards from the corona tip on both sides and symmetrically charges the surface, while the discharge is sustained by the sheath accelerated secondary electrons. The discharge is terminated when the electric field for the SIW is reduced by virtue of the distance the SIW has traveled from the corona electrode. When the dielectric surface is in motion, surface charges and the potential they produce are translated away from the corona wire. The voltage between the corona electrode and the incoming uncharged surface rebounds, and an electron avalanche is re-ignited on one side of the blade. The corona discharge process then repeats to form an oscillatory charging pattern. The charging pattern can be made less oscillatory by using a fast-moving surface or a gas mixture capable of continuously providing seed electrons to maintain the discharge.

ACKNOWLEDGMENTS

Work was supported by Hewlett-Packard Research Labs.

[1]S. F. Miralaï, E. Monette, R. Bartnikas, G. Czeremuszkin, M. Latrèche, and M. R. Wertheimer, Plasmas Polym. **5**, 63 (2000).
[2]F. Massines, G. Gouda, N. Gherardi, M. Duran, and E. Croquesel, Plasmas Polym. **6**, 35 (2001).
[3]L.-A. O'Hare, S. Leadley, and B. Parbhoo, Surf. Interface Anal. **33**, 335 (2002).
[4]S. Guimond, I. Radu, G. Czeremuszkin, D. J. Carlsson, and M. R. Wertheimer, Plasmas Polym. **7**, 71 (2002).
[5]M. Sira, D. Trunec, P. Stahel, V. Bursikova, Z. Navratil, and J. Bursik, J. Phys. D: Appl. Phys. **38**, 621 (2005).
[6]Q. Zhang, C. Wang, Y. Babukutty, T. Ohyama, M. Kogoma, and M. Kodama, J. Biomed. Mater. Res. **60**, 502 (2002).
[7]C. Geβner, V. Bartels, T. Betker, U. Matucha, C. Penache, and C.-P. Klages, Thin Solid Films **459**, 118 (2004).
[8]P.-L. Girard-Lauriault, F. Mwale, M. Iordanova, C. Demers, P. Desjardins, and M. R. Wertheimer, Plasma Processs Polym. **2**, 263 (2005).
[9]C. Sarra-Bournet, S. Turgeon, D. Mantovani, and G. Laroche, J. Phys. D: Appl. Phys. **39**, 3461 (2006).
[10]M. H. Lee, N. J. Leoni, H. Birecki, and O. Gila, U.S. patent 2011/0216126 (8 September 2011).
[11]O. Gila, N. J. Leoni, and J. Nielsen, U.S. patent 2012/0272896 (1 November 2012).
[12]J. Kurokawa, K. Nojima, and N. Sohmiya, U.S. patent 5,499,078 (12 March 1996).
[13]D. M. Pai and B. E. Springett, Rev. Mod. Phys. **65**, 163 (1993).
[14]L. B. Schein, J. Vac. Sci. Technol., A **25**, 1256 (2007).
[15]C. B. Duke, J. Noolandi, and T. Thieret, Surf. Sci. **500**, 1005 (2002).
[16]R. M. Schaffert, *Electrophotography* (Focal Press, London, 1965).
[17]J. S. Chang, P. A. Lawless, and T. Yamamoto, IEEE Trans. Plasma Sci. **19**, 1152 (1991).
[18]E. M. van Veldhuizen and W. R. Rutgers, in *Proceedings of Frontiers in Low Temperature Plasma Diagnostics IV, Limburg* (NL) (Department of Applied Physics, University of Technology, Eindhoven, 2001).
[19]B. Lay, R. S. Moss, S. Rauf, and M. J. Kushner, Plasma Sources Sci. Technol. **12**, 8 (2003).
[20]J.-C. Wang, N. Leoni, H. Birecki, O. Gila, and M. J. Kushner, J. Appl. Phys. **113**, 033301 (2013).
[21]D. L. Scharfetter and H. K. Gummel, IEEE Trans. Electron Devices **16**, 64 (1969).
[22]R. Dorai, "Modeling of atmospheric pressure plasma processing of gases and surfaces," Ph.D. thesis (University of Illinois, 2002), see http://uigelz.eecs.umich.edu/theses.html.
[23]Y. Akishev, M. Grushin, V. Karalnik, A. Petryakov, and N. Trushkin, J. Phys. D: Appl. Phys. **43**, 215202 (2010).
[24]S. Celestin, K. Allegraud, G. Canes-Boussard, N. Leick, O. Guaitella, and A. Rousseau, IEEE Trans. Plasma Sci. **36**, 1326 (2008).
[25]S. Celestin, G. Canes-Boussard, O. Guaitella, A. Bourdon, and A. Rousseau, J. Phys. D: Appl. Phys. **41**, 205214 (2008).
[26]S. Celestin, Z. Bonaventura, O. Guaitella, A. Rousseau, and A. Bourdon, Eur. Phys. J.: Appl. Phys. **47**, 22810 (2009).
[27]F. Pechereau, J. Jansky, and A. Bourdon, Plasma Sources Sci. Technol. **21**, 055011 (2012).
[28]D. S. Antao, D. A. Staack, A. Fridman, and B. Farouk, Plasma Sources Sci. Technol. **18**, 035016 (2009).
[29]Y. P. Raizer, *Gas Discharge Physics* (Springer, Berlin, 1991).
[30]M. Goldman, A. Goldman, and R. S. Sigmond, Pure Appl. Chem. **57**, 1353 (1985).
[31]J. Chen and J. H. Davidson, Plasma Chem. Plasma Process. **23**, 83 (2003).